Structural Studies of Allelic Diversity of the MHC Class I Homolog MIC-B, a Stress-Inducible Ligand for the Activating Immunoreceptor NKG2D¹

Margaret A. Holmes,²* Pingwei Li,²* Effie W. Petersdorf,^{†‡} and Roland K. Strong³*

MIC-A and MIC-B are distant MHC class I homologs that serve as stress-inducible Ags on epithelial and epithelially derived cells. They are ligands for the widely expressed activating immunoreceptor NKG2D. To define the structural and functional consequences of sequence differences between MIC-A and MIC-B and between alleles of MIC-A and alleles of MIC-B, we determined the crystal structure of one allele of human MIC-B. Comparisons between the two previously reported MIC-A crystal structures and the MIC-B crystal structure show that, as expected, MIC-B is very similar in structure to MIC-A and likely interacts with NKG2D in an analogous manner. The interdomain flexibility observed in the MIC-A structures, a feature unique to MIC proteins among MHC class I proteins and homologs, is also displayed by MIC-B, with an interdomain relationship intermediate between the two examples of MIC-A structures. Mapping sequence variations onto the structures of MIC-A and MIC-B reveals patterns completely distinct from those displayed by classical MHC class I proteins, with a number of substitutions falling on positions likely to affect interactions with NKG2D, but with other positions lying distant from the NKG2D binding sites or buried within the core of the proteins. *The Journal of Immunology*, 2002, 169: 1395–1400.

he proteins encoded by the classical HLA class I loci in the MHC (HLA-A, HLA-B, and HLA-C) are involved in peptide transport and presentation to Ag-specific CD8⁺ T cells (1). The ability of these proteins to bind diverse peptide Ags and TCRs is reflected in the wide variation in the frequency of individual HLA alleles and haplotypes in the population and their extraordinary polymorphism, which maps predominately to residues lining the peptide binding groove and to the surfaces interacting with TCRs (2). The nonclassical HLA loci (HLA-E, HLA-F, and HLA-G), involved in other types of immune responses, are considerably less polymorphic (3-5). Classical MHC class I proteins are ubiquitously expressed, while the nonclassical molecules have much more restricted tissue distributions. Additional loci encoding MHC class I homologs have been identified within the MHC, including the distantly related MHC class I chain-related loci MIC-A and MIC-B, which are conserved in most mammals except rodents (6-8).

Comparable to the nonclassical class I molecules, MIC-A and MIC-B are induced only in response to cellular stress signals on limited cell types, essentially restricted to intestinal epithelium and epithelially derived tumors (8, 9). While MIC-A and MIC-B are quite similar to each other (84% identical) (7, 10), they have diverged significantly from the MHC class I family as a whole, with identities of 28–35% compared domain-by-domain when aligned

Divisions of *Basic Sciences and [†]Clinical Research, Fred Hutchinson Cancer Research Center, Seattle, WA 98109; and [‡]University of Washington School of Medicine, Seattle, WA 98195

Received for publication February 27, 2002. Accepted for publication May 29, 2002.

The costs of publication of this article were defrayed in part by the payment of page charges. This article must therefore be hereby marked *advertisement* in accordance with 18 U.S.C. Section 1734 solely to indicate this fact.

with human MHC class I proteins. Unlike classical and nonclassical MHC class I proteins and most MHC class I homologs, MIC proteins do not require either peptide or β_2 -microglobulin for folding, stability, or cell surface expression (8, 11). MIC-A and MIC-B are ligands for the C-type lectin-like activating immunoreceptor NKG2D (6–8), whose expression was first recognized on NK cells but was subsequently found on CD8⁺ $\alpha\beta$ T cells, $\gamma\delta$ T cells, and macrophages, making it one of the most widely distributed NK cell receptors currently described (12, 13). NKG2D-MIC recognition events stimulate effector responses from NK cells and $\gamma\delta$ T cells and may positively modulate CD8⁺ $\alpha\beta$ T cell responses, thus serving a costimulatory function (12, 14). Ligand engagement of NKG2D is signaled through recruitment of phosphatidylinositol 3-kinase through the adapter molecule DAP10 (13, 15).

MIC-A and MIC-B are highly polymorphic, with >50 MIC-A and 13 MIC-B alleles recognized, numbers that continue to increase (reviewed in Ref. 16). There are numerous polymorphisms spread over the extracellular domains of the proteins, predominantly the result of single amino acid substitutions that generate dimorphic positions (Fig. 1). Many of these changes are nonconservative. This contrasts with the classical MHC class I polymorphisms, in both the relative positions of the polymorphisms in the sequence and the number of different amino acids at a polymorphic site, which can be numerous. A number of diseases have been reported to be associated with *MIC* gene polymorphisms, including ankylosing spondylitis, Behçet's disease, psoriasis, type I diabetes, and Addison's disease, among others, but none definitively (reviewed in Ref. 16).

Crystal structures of MIC-A, alone (11) and in complex with NKG2D (17), revealed a very distorted example of an MHC class I platform domain (here, we use the terminology "platform domain" to refer to the single structural folding unit consisting of the $\alpha 1$ and $\alpha 2$ domains of the MHC class I H chain). This domain comprises two long, roughly parallel α helices, interrupted by bends, arranged on an eight-stranded β -sheet in MHC class I proteins. These α helices define the peptide binding groove in MHC

 $^{^{1}}$ This work was supported by National Institutes of Health Grants AI48675 (to R.K.S.) and CA72978 (to E.W.P.).

² M.A.H. and P.L. contributed equally to this work.

³ Address correspondence and reprint requests to Dr. Roland K. Strong, Division of Basic Sciences, Fred Hutchinson Cancer Research Center, 1100 Fairview Avenue North, Seattle, WA 98109. E-mail address: rstrong@fhcrc.org

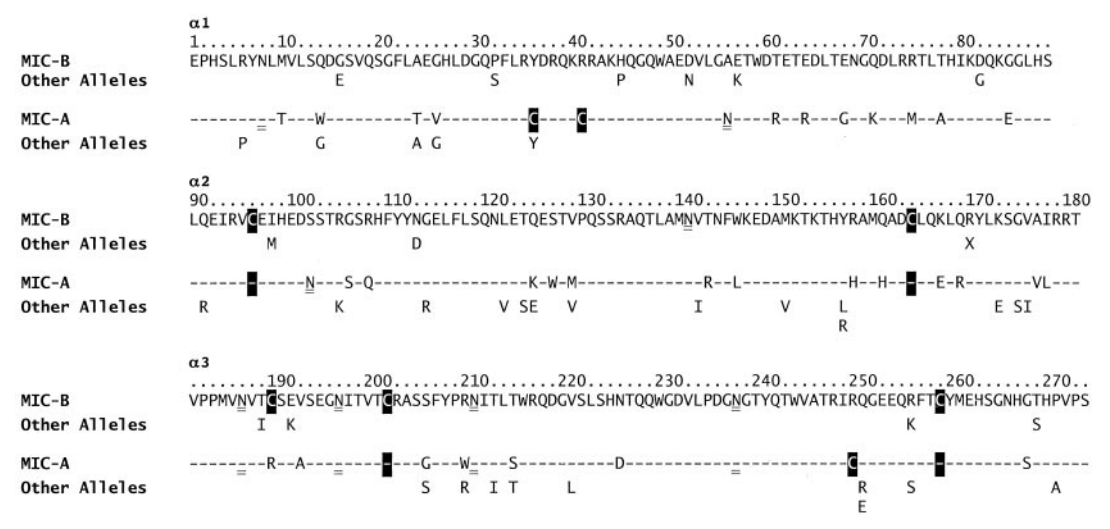


FIGURE 1. Sequences of MIC-A and MIC-B alleles. The alignment of the sequences of MIC-A and MIC-B, both from the crystal structures, are shown, broken down by domain (7, 10). Dashes indicate identities between the MIC-B and MIC-A sequences. Sequence substitutions present in other alleles are shown below the corresponding sequence (an X indicates a premature stop codon) (Ref. 16 and E. W. Petersdorf, unpublished results). Cysteines are shown on a black background; potentially glycosylated asparagine residues are double-underlined.

class I homologs that bind peptides. Although a pocket was apparent in the center of the MIC-A platform domain, likely a remnant of a peptide binding groove, it was too small to allow for the binding of anything larger than the equivalent of a three- or four-residue peptide. This, plus the polar character of the lining of the pocket and the lack of any electron density not accounted for by protein atoms in the structure, led to the conclusion that MIC-A does not bind any peptide or other small-molecule ligand (11). The platform and $\alpha 3$ domains of MIC-A are joined through a flexible linker, allowing considerable interdomain flexibility, a feature unique to MIC-A among MHC class I proteins and homologs.

We have determined the 2.5-Å resolution crystal structure of MIC-B by multiwavelength anomalous dispersion (MAD)⁴ phasing to rationalize the observed sequence polymorphism in the *MIC-A* and *MIC-B* loci, and we attempt to correlate sequence substitutions between MIC-A and MIC-B alleles with structural features on these molecules to tease out potential functional relevancies.

Materials and Methods

The extracellular domain of MIC-B (allele 005; residues 1-274 plus an N-terminal initiator methionine residue and a C-terminal six-histidine metalaffinity purification tag) was expressed in bacteria and refolded from inclusion bodies using a variation of the method developed for MIC-A (11). Proper folding was assayed by solution monodispersivity of the purified, concentrated protein, as determined by the presence of a single disulfidebonded species by nonreducing PAGE analysis, size exclusion chromatography, and dynamic light scattering. A selenomethionine derivative was prepared by the method of Doublié (18). Crystals were grown by hangingdrop vapor diffusion at 22°C from a protein solution at 10-15 mg/ml, mixed 1:1 with a well solution of 1.2 M (NH₄)₂SO₄, 50 mM Tris (pH 8.5). The space group was $P42_12$, a = b = 81.7 Å and c = 86.6 Å, with a single monomer in the asymmetric unit. Size exclusion chromatography analysis showed that the engineered, soluble MIC-B is monomeric in solution. Crystals were cryopreserved by stepwise transfer to a mother liquor that included 40% sucrose.

Diffraction data from native and selenomethionine crystals were collected at the Advanced Light Source (Lawrence Berkeley National Laboratory, Berkeley, CA), beamline 5.0.2, using a charge-coupled device, and were reduced with HKL (Ref. 19; Table I). Using the CNS software package (20), MAD phases were calculated from five of the seven possible

selenium sites in MIC-B located by automated Patterson search. The initial electron density map calculated with these phases was clear and readily interpretable. After solvent flipping and phase extension in CNS, the homologous structure of MIC-A (11) (Brookhaven Protein Data Bank (PDB) (21), accession no. 1HYR) was positioned in the electron density map for use as a scaffold during building but was not used to provide additional phase information.

Rebuilding, using O (22) and xfit (23), alternated with cycles of positional refinement (using the mlhl and mlf target functions) and temperature factor refinement, initially with group Bs but finally with individual Bs, in CNS (Table II). The only solvent molecules included in the structure are five sulfates. Due to poor quality density, the side chain of Lys⁴⁰ has been modeled without the two terminal atoms, and residues 148–154, 191, 229, and 248 have been modeled as either glycine or alanine. Coordinates have been deposited in the PDB (accession no. 1JE6).

Results

Crystal structure of MIC-B

Like the H chain of other MHC class I proteins and homologs and MIC-A, the fold of MIC-B consists of two structural domains: the $\alpha 1\alpha 2$ platform domain and the C-type Ig-like $\alpha 3$ domain (Fig. 2A). In all MHC class I protein and homolog structures to date, these domains display an interdomain relationship that varies by $<30^\circ$. However, the two MIC-A structures, alone (11) and in complex with the C-type lectin-like NK cell receptor NKG2D (17), showed an unprecedented degree of interdomain flexibility (Fig. 2A). This feature is shared by MIC-B, which displays a platform- $\alpha 3$ domain angle intermediate between the MIC-A structures (Fig. 2A). Therefore, the crystal structure of MIC-B reinforces the conclusion, based on the MIC-A structures, that MIC proteins, unique among MHC class I proteins and homologs, have extremely flexibly linked H chain domains.

As in the crystal structures of MIC-A and consistent with the MHC class I family, the platform domain consists of two α helices arranged on an eight-stranded antiparallel β -sheet. However, in MIC-A crystallized in the absence of receptor, 10 residues (152–161) in the center section of the helical element in the α 2 domain (corresponding to helix 2a in MHC class I proteins) are disordered and presumed to form an extended, flexible loop. These residues are ordered in MIC-A when complexed with NKG2D, forming two additional turns of α helix and a stretch of coil (Fig. 2A). Ordering of this loop in the complex is due to contacts between MIC-A residues in this loop and residues of the immunoreceptor. Flexible

⁴ Abbreviations used in this paper: MAD, multiwavelength anomalous dispersion; rmsd, root mean square deviation; ZAG, $Zn-\alpha_2$ -glycoprotein.

The Journal of Immunology 1397

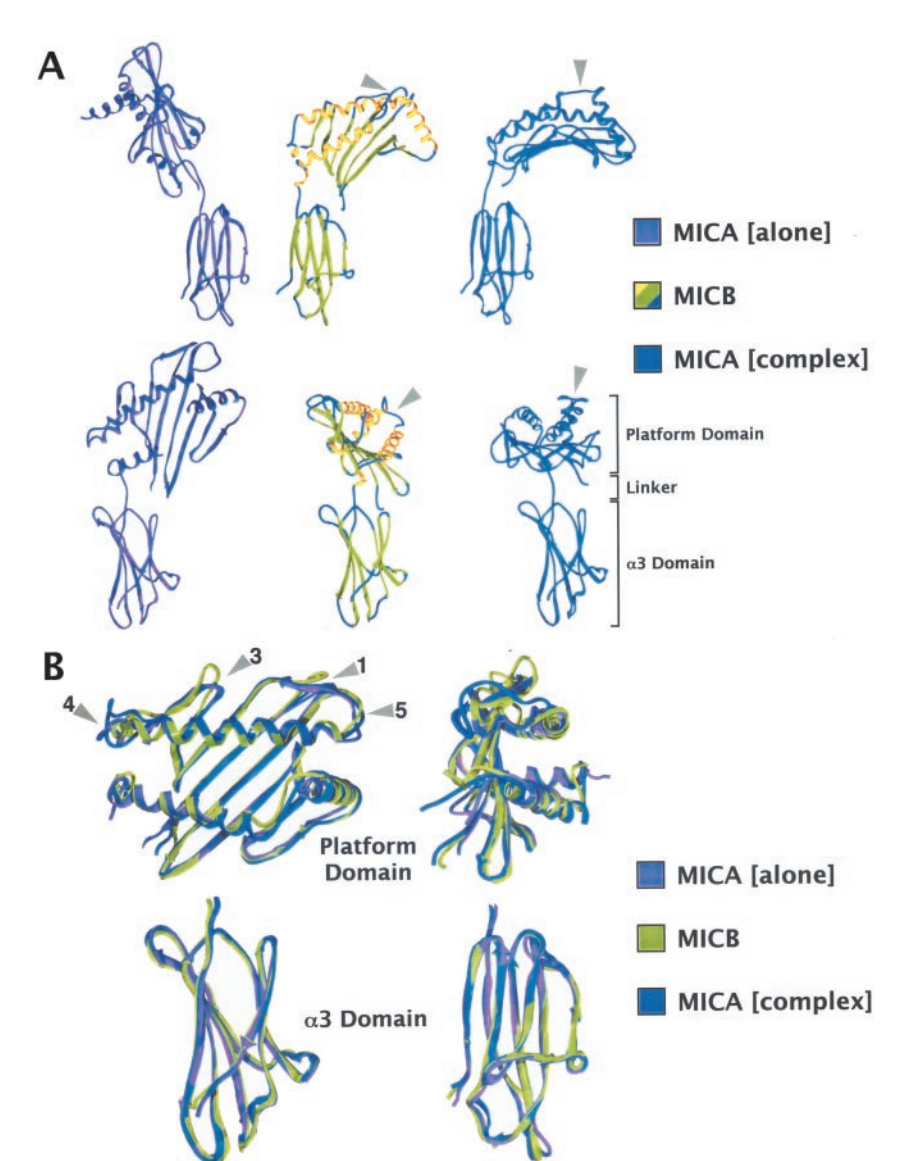


FIGURE 2. Structures of MIC-A and MIC-B. A, Ribbon representations of the backbone structures of MIC-A (left), crystallized on its own (PDB accession no. 1B3J), MIC-B (center), and MIC-A (right), extracted from the complex structure with NKG2D (PDB accession no. 1HYR). Structures in the lower row are rotated by 90° around the vertical axis from structures in the upper row. Secondary structure elements are indicated (α helices as springs, β -strands as arrows, and coil as tubes) and are in yellow, green, and blue, respectively, for MIC-B. The loops in MIC-B and MIC-A from the complex corresponding to the disordered loop in MIC-A crystallized alone are indicated by the gray arrows. B, Superpositions of the platform domains (top) and α 3 domains (bottom) of the three MIC structures are shown. Structures on the right are rotated by 90° around the vertical axis from structures on the left. Numbered arrows indicate loops discussed in Results.

loops have also been observed in the structure of the murine MHC class I homolog H-2T22, for example, but corresponding to different secondary structure elements (24).

In MIC-B, the residues corresponding to the MIC-A disordered loop are ordered in a structure similar to what is seen in the MIC-A-NKG2D complex (Fig. 2A). However, the electron density corresponding to these residues is poorer, as reflected in elevated B factors and the necessity to model a number of these residues as either glycines or alanines. This likely indicates that the MIC-B loop displays some conformational flexibility, although not as much as is seen in MIC-A. It is not immediately apparent what accounts for this increased order, because many of the residues involved in interactions between the loop and the rest of the protein are conserved between MIC-A and MIC-B. The substitution of tryptophan (MIC-B) for leucine (MIC-A) at position 146 may affect loop stability by altering the packing of Tyr157 against the hydrophobic core of the protein, as might the substitution of arginine (MIC-B) for glutamine (MIC-A) at position 108. These residues form part of the surface underlying the loop. While none of the residues within this loop make direct, stabilizing contacts to other molecules in the crystal lattice, neighboring molecules do approach closely enough to severely limit the range of conformations available to this loop in the MIC-B crystal structure.

The structure of the platform domain of MIC-B is more similar to the platform domain of MIC-A in the complex with NKG2D (root mean square deviation (rmsd) of 1.45 Å on 160 C α s) than the platform domain of MIC-A crystallized alone (rmsd of 1.79 Å on 150 Cαs, excluding residues corresponding to the disordered loop). The largest differences in the structures occur in loops surrounding the platform domain, mostly in the $\alpha 1$ subdomain: movements of up to 6.6 Å in residues 80-86 (Fig. 2B, loop 5) and up to 4.3 Å in residues 14–16 (Fig. 2B, loop 1), and substantial rearrangements in residues 45-59 (Fig. 2B, loop 4). Loop 4 is more helical in MIC-B and free MIC-A than in MIC-A in the complex with NKG2D, where it forms an extended, poorly ordered loop. MIC-B lacks the noncanonical disulfide bond (Cys³⁶-Cys⁴¹; a disulfide bond not conserved in MHC class I proteins and homologs) present in MIC-A that closes off a four-residue loop (Fig. 2B, loop 3). In MIC-B, this loop is extended by two residues (Q39 and K40) and curls downward, away from the putative location of NKG2D in a complex with MIC-B. The result is that, while the sequences of MIC-A and MIC-B are highly conserved in this region (residues 38-51 in MIC-B, ROKRRAKPOGOWAE; in MIC-A, ROKCRA KPQGQWAE), the backbones are out of register by two residues in the region of the β -strand between loops 3 and 4. The register is not clearly restored to matching until after loop 4 (residue 59).

Table I. Data collection and phasing statistics^a

	Native	SeMet λ_1	SeMet λ_2	SeMet λ_3
Wavelength (Å)	1.100	0.9795	0.9793	0.9567
Resolution (Å)	2.50	2.70	2.90	2.90
High resolution shell (Å)	2.59 to 2.50	2.80 to 2.70	3.00 to 2.90	3.00 to 2.90
Unique reflections	10,656	8,597	6,869	6,895
Redundancy	10.1	15.6	13.5	6.66
Completeness (%)	99.6 (100.0)	99.6 (100.0)	97.7 (98.2)	97.6 (98.2)
$\langle I/\sigma(I)\rangle$	49.9 (6.8)	37.0 (6.1)	35.8 (7.7)	22.3 (4.3)
R _{sym} (%)	6.2 (35.3)	7.9 (40.5)	8.6 (29.3)	8.0 (30.8)
Anomalous difference (%)		4.81	5.80	5.40
Phasing power (centrics/acentrics)		1.71/1.61	1.74/1.44	1.09/0.83

 $[^]a$ Values for the highest resolution shell are shown in parentheses. $R_{\mathrm{sym}} = \Sigma |I - \langle I \rangle|/\Sigma \langle I \rangle$ where I is the observed intensity and $\langle I \rangle$ is the mean intensity of multiple observations of symmetry-related reflections. Phasing power = $\langle |F_{\mathrm{H}}|/E \rangle$ where F_{H} is the heavy atom structure factor amplitude and E is the residual lack-of-closure error. Overall figure-of-merit (20 to 2.90 Å): 58%.

Despite this difference between MIC structures, we are confident that we have modeled this loop in MIC-B accurately; the initial, MAD-phased electron density map is clear and unambiguous in this region. The $\alpha 3$ domains are closer in structure (rmsd of MIC-B onto free MIC-A, 0.97 Å on 94 C α s; MIC-B onto complex MIC-A, 0.83 Å on 94 C α s) (Fig. 2B). The largest differences occur in two loops (residues 192–196 and 236–238), likely the result of different environments for these loops in the three crystal forms.

As in the structure of MIC-A in the complex with NKG2D, there is a pocket in the center of the platform domain (as shown in Fig. 3, the pocket is centered within the NKG2D contact surfaces) similar in size and shape to the ligand binding pocket of $Zn-\alpha_2$ -glycoprotein (ZAG), another MHC class I homolog (25). However, unlike ZAG, the surface lining this pocket is not particularly hydrophobic and is, indeed, lined with a number of side chains from charged or polar residues: N69, T76, E92, R94, R108, and W146. As in the MIC-A structures, and unlike ZAG, there is no electron density in MIC-B difference Fourier syntheses not accounted for by protein or solvent atoms. Attempts to drive the binding of a hypothetical ligand by dialyzing MIC-B against conditioned medium and mammalian cell lysates before crystallization fail to alter the appearance of derived electron density maps (data not shown), suggesting that this pocket is a nonfunctional remnant of the peptide binding groove of classical MHC class I proteins and does not bind any small-molecule ligand. These soaking experiments were predicated on the expectation that a hypothetical MIC ligand would be soluble, based on the polar character of the lining of the pocket.

Discussion

Structural consequences of allelic substitutions in MIC-A and MIC-B: implications for receptor binding

An analysis of amino acid substitutions between the alleles of MIC-A and MIC-B used for the crystallographic analysis involved in the binding of NKG2D reveals six differences: R64E (E in MIC-B), K71Q, M75R, A78T, D149E, and H158R. To map the NKG2D receptor binding footprint onto the structure of MIC-B, the platform domain of MIC-B was docked onto the platform domain of MIC-A in the MIC-A-NKG2D complex crystal structure (Fig. 3). In this crudely modeled MIC-B-NKG2D complex, only one potentially bad contact is revealed: R75 in MIC-B, clashing with A193, K197, and Y199 in NKG2D. However, the flexible arginine side chain could easily adopt a conformation that would avoid steric clashes. Therefore, we predict that MIC-B interacts with NKG2D in a manner very similar to the MIC-A-NKG2D complex. Preordering of the loop in MIC-B corresponding to the disordered loop in the α 2 domain of MIC-A would also be predicted to reduce

the unusually slow on-rate observed for MIC-A-NKG2D binding (17) by reducing the activation energy required to reach the binding transition state, with a concomitant increase in overall affinity.

However, mapping of the sequence differences observed between known MIC-A and MIC-B alleles (Figs. 1 and 3) yields a much less clear picture. The substitutions range from quite conservative (R/K) to quite dramatic (P/H), from residues very close to NKG2D contact residues to quite distant from the binding site (in this analysis, we focus only on substitutions mapping to the platform domain because the \alpha3 domain has been shown by domain swapping experiments not to play a direct role in any intermolecular recognition event (14)). The positions of the substitutions are fairly evenly distributed over the surface of the domain, although they cluster somewhat to the α 2 domain in MIC-A and to the helix side of the platform domain in MIC-B. In MIC-A, only one known allelic substitution maps to an NKG2D contact residue, at position 156, where histidine, leucine, or arginine are found among different MIC-A alleles. The side chains of these residues are different enough to expect an effect on the affinity for NKG2D and would likely involve alterations in the inter- and intramolecular hydrogen bond networks observed in the structure.

Of the remaining substitutions, many are distant from NKG2D and would not be predicted to have a dramatic affect on the complex affinity or the structure of MIC-A (positions 14, 24, 91, 105,

Table II. Refinement statistics^a

Refinement		
Resolution (Å)	20 to 2.50	
Reflections (all $F > 0$;	9385/1074	
working/test)		
Protein/sulfate atoms	2171/20	
$R_{\rm cryst}/R_{\rm free}$ (%)	25.5/29.8	
Average B factor (Å ²)	43.6	
Wilson intercept (Å ²)	41.2	
Cross-validated σ_{A}	0.46	
coordinate error (Å)		
Geometry (rmsd from ideality)		
Bond length (Å)	0.009	
Bond angles (degrees)	1.7	
Ramachandran		
Most favored (%)	84.7	
Additional allowed (%)	13.2	
Generously allowed (%)	2.1	
Disallowed (%)		

 $[^]aR_{\text{Cryst}}$, $R_{\text{Free}} = \sum \|F_{\text{obs}}\| - |F_{\text{calc}}\|/\Sigma|F_{\text{obs}}|$ where F_{obs} and F_{calc} are the observed and calculated structure factor amplitudes. Ramachandran values were calculated with PROCHECK (26). R_{Free} is calculated from a randomly chosen 10% of the reflections excluded from refinement (27).

The Journal of Immunology 1399

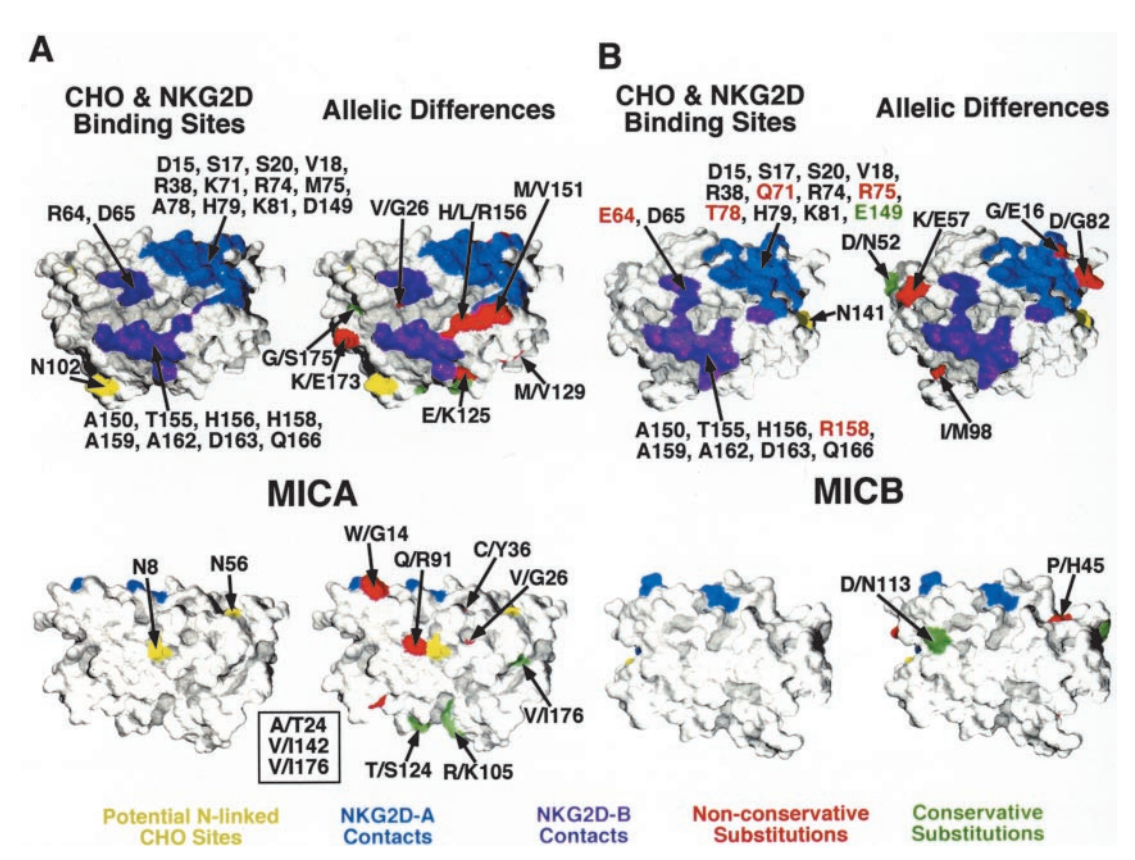


FIGURE 3. Mapping of receptor binding sites, potential carbohydrate sites, and MIC sequence variations to MIC molecular surfaces. Molecular surfaces of the platform domains of MIC-A (A) and MIC-B (B) are shown, with views from above (the NKG2D binding side) shown in the *upper row* and views from below (rotated by 180°) shown in the *lower row*. Each surface is shown twice, once on the *left* side of each frame and again on the *right* side, with different surface features highlighted and labeled on each side. The molecular surface of asparagine residues at potential N-linked glycosylation sites is yellow and labeled in the left side views. The molecular surface of MIC residues that contact the NKG2D-A half of the receptor are blue; the surface of NKG2D-B half-site contact residues is purple. Contact residues within each half-site are labeled in the left views. For MIC-A, NKG2D contact residues were identified on the basis of the crystal structure of the complex; for MIC-B, the contact residues were assigned on the basis of substituting the structure of MIC-B for MIC-A in the complex structure to serve as a simplistic model of a MIC-B-NKG2D complex. In B, on the *left side*, sequence differences between MIC-A and MIC-B NKG2D contact residues are highlighted, with conservative substitution labels in green and nonconservative substitution labels in red. The surfaces of residues at polymorphic positions in MIC-A (A) and MIC-B (B) are green (conservative) or red (nonconservative) and are labeled in the *right* views. Allelic substitutions in MIC-A residues that present no appreciable accessible surface area are indicated within the boxed area.

124, 125, 129, and 173). However, one of these seemingly innocuous substitutions, M/V129, a conservative substitution that has no atom closer than 21 Å to any atom of NKG2D, has been experimentally shown to have a 30-fold affect on the affinity for NKG2D (Ref. 28 and B. E. Willcox and R. K. Strong, unpublished results), demonstrating a caveat of this type of analysis. Nevertheless, a number of the MIC-A substitutions would likely impose minor rearrangements in surrounding MIC-A residues (positions 26, 142, 175, and 176), but none of these would be predicted to affect the NKG2D complex. The M/V151 substitution lies very close to the NKG2D interface, but is not involved in a direct contact, nor would a methionine/valine substitution obviously result in a conformational change. C/Y36 involves a noncanonical disulfide bond not present in other MHC class I homologs or MIC-B. The loop at the edge of the platform domain encompassing this position (Fig. 2B, loop 3) is quite different between the MIC-A and MIC-B structures but is not involved in any direct contacts with NKG2D. Therefore, this substitution is again not predicted to affect the MIC-NKG2D interaction. Using similar arguments, the observed allelic substitutions at positions 52, 57, 82, 98, and 113 would also not be predicted to significantly affect the structure of MIC-B or its interaction with NKG2D, while substitutions at positions 16 and 45 would likely result in local changes to the structure of MIC-B but are distant enough from NKG2D residues to not affect binding.

Conclusions

Sequence polymorphisms between MIC-A and MIC-B alleles and sequence differences between MIC-A and MIC-B do not cluster, defining potential ligand or receptor binding sites, as in classical MHC class I proteins. Indeed, these substitutions are distributed over the surface of the molecules and between solvent exposed and buried residues. While several of the sequence variations are predicted to affect NKG2D interactions and thus may modulate NKG2D-mediated cellular responses, many of the substitutions are not predicted to affect NKG2D binding. However, these positions may map to as-yet-unidentified receptor interaction sites.

Acknowledgments

We thank L. Hung, G. McDermott, and T. Earnest (Advanced Light Source, Lawrence Berkeley National Laboratory) for assistance with diffraction data collection and Jordan Devereaux for assistance with the MIC-B soaking experiments.

References

- Bjorkman, P. J., and P. Parham. 1990. Structure, function and diversity of class I major histocompatibility complex molecules. *Annu. Rev. Biochem.* 90:253.
- Mason, P. M., and P. Parham. 1998. HLA class I region sequences, 1998. Tissue Antigens 51:417.
- Geraghty, D. E., B. H. Koller, and H. T. Orr. 1987. A human major histocompatibility complex class I gene that encodes a protein with a shortened cytoplasmic segment. *Proc. Natl. Acad. Sci. USA* 84:9145.

- Koller, B. H., D. E. Geraghty, Y. Shimizu, R. DeMars, and H. T. Orr. 1988. HLA-E: a novel HLA class I gene expressed in resting T lymphocytes. *J. Immunol.* 141:897.
- Geraghty, D. E., X. H. Wei, H. T. Orr, and B. H. Koller. 1990. Human leukocyte antigen F (HLA-F): an expressed HLA gene composed of a class I coding sequence linked to a novel transcribed repetitive element. J. Exp. Med. 171:1.
- Bahram, S., M. Bresnahan, D. E. Geraghty, and T. A. Spies. 1994. A second lineage of mammalian major histocompatibility complex class I genes. *Proc.* Natl. Acad. Sci. USA 91:6259.
- 7. Bahram, S., and T. A. Spies. 1996. Nucleotide sequence of a human *MHC* class I *MICB* cDNA. *Immunogenetics* 43:230.
- Groh, V., S. Bahram, S. Bauer, A. Herman, M. Beauchamp, and T. Spies. 1996. Cell stress-regulated human major histocompatibility complex class I gene expressed in gastrointestinal epithelium. *Proc. Natl. Acad. Sci. USA* 93:12445.
- Groh, V., R. Rhinehart, H. Secrist, S. Bauer, K. H. Grabstein, and T. Spies. 1999. Broad tumor-associated expression and recognition by tumor-derived γδ T cells of MICA and MICB. Proc. Natl. Acad. Sci. USA 96:6879.
- Bahram, S., N. Mizuki, H. Inoko, and T. A. Spies. 1996. Nucleotide sequence of the human MHC class I MICA gene. Immunogenetics 44:80.
- Li, P., S. T. Willie, S. Bauer, D. L. Morris, T. Spies, and R. K. Strong. 1999. Crystal structure of the MHC class I homolog MIC-A, a γδ T cell ligand. Immunity 10:577.
- Bauer, S., V. Groh, J. Wu, A. Steinle, J. H. Phillips, L. L. Lanier, and T. Spies. 1999. Activation of NK cells and T cells by NKG2D, a receptor for stress-inducible MICA. Science 285:727.
- Wu, J., Y. Song, A. B. Bakker, S. Bauer, T. Spies, L. L. Lanier, and J. H. Phillips. 1999. An activating immunoreceptor complex formed by NKG2D and DAP10. Science 285:730.
- Groh, V., A. Steinle, S. Bauer, and T. Spies. 1998. Recognition of stress-induced MHC molecules by intestinal epithelial γδ T cells. Science 279:1737.
- Wu, J., H. Cherwinski, T. Spies, J. H. Phillips, and L. L. Lanier. 2000. DAP10 and DAP12 form distinct, but functionally cooperative, receptor complexes in natural killer cells. J. Exp. Med. 192:1059.

- Stephens, H. A. 2001. MICA and MICB genes: can the enigma of their polymorphism be resolved? *Trends Immunol.* 22:378.
- Li, P., D. L. Morris, B. E. Willcox, A. Steinle, T. Spies, and R. K. Strong. 2001.
 Complex structure of the activating immunoreceptor NKG2D and its MHC class I-like ligand MICA. *Nat. Immunol.* 2:443.
- Doublié, S. 1997. Preparation of selenomethionyl proteins for phase determination. Methods Enzymol. 276:523.
- Otwinowski, Z., and W. Minor. 1997. Processing of x-ray diffraction data collected in oscillation mode. In *Methods in Enzymology*, Vol. 276. C. W. Carter, Jr., and R. M. Sweet, eds. Academic, New York, p. 307.
- Brünger, A. T., P. D. Adams, G. M. Clore, W. L. DeLano, P. Gros, R. W. Grosse-Kunstleve, J.-S. Jiang, J. Kuszewski, M. Nilges, N. S. Pannu, et al. 1998. Crystallography & NMR System: a new software suite for macromolecular structure determination. Acta Crystallogr. D 54:905.
- Berman, H. M., J. Westbrook, Z. Feng, G. Gilliland, T. N. Bhat, H. Weissig, I. N. Shindyalov, and P. E. Bourne. 2000. The Protein Data Bank. *Nucleic Acids Res.* 28:235.
- Jones, T. A., and M. Kjeldgaard. 1997. Electron density map interpretation. Methods Enzymol. 277:173.
- McRee, D. E. 1992. XtalView: a visual protein crystallographic software system for XII/XView. J. Mol. Graphics 10:44.
- Wingren, C., M. P. Crowley, M. Degano, Y.-H. Chien, and I. A. Wilson. 2000. Crystal structure of a γδ T cell receptor ligand T22: a truncated MHC-like fold. Science 287:310.
- Sanchez, L. M., A. J. Chirino, and P. J. Bjorkman. 1999. Crystal structure of human ZAG, a fat-depleting factor related to MHC molecules. Science 283:1914.
- Laskowski, R. A., M. W. MacArthur, E. G. Hutchinson, and J. M. Thornton. 1992. PROCHECK: a program to check the stereochemical quality of protein structures. J. Appl. Crystallogr. 26:283.
- Brünger, A. T. 1992. Free R value: a novel statistical quantity for assessing the accuracy of crystal structures. *Nature* 355:472.
- Steinle, A., P. Li, D. L. Morris, V. Groh, L. L. Lanier, R. K. Strong, and T. Spies. 2001. Interactions of human NKG2D with its ligands MICA, MICB, and homologs of the mouse RAE-1 protein family. *Immunogenetics* 53:279.